RSC Advances

PAPER

View Article Online
View Journal | View Issue

Cite this: *RSC Adv.*, 2016, **6**, 102444

Heterostructured g-C_3N_4/Ag/TiO_2 nanocomposites for enhancing the photoelectric conversion efficiency of spiro-OMeTAD-based solid-state dye-sensitized solar cells

Haoran Yan,[a] Xin Tian,[a] Yongxin Pang,[b] Bo Feng,[a] Ke Duan,[a] Zuowan Zhou,[a] Jie Weng[a] and Jianxin Wang*[a]

Received 25th July 2016
Accepted 13th October 2016

DOI: 10.1039/c6ra18758g

www.rsc.org/advances

In this study, solid state dye-sensitized solar cells (ss-DSSCs) were fabricated with g-C_3N_4 and Ag co-modified TiO_2 nanoparticles as photoanode materials. Devices with spiro-OMeTAD as hole transport materials (HTMs) showed a high power conversion efficiency (PCEs) of 6.22%. For the heterostructured g-C_3N_4/Ag/TiO_2 nanocomposites, Ag nanoparticles were deposited as an electron-conduction bridge between the TiO_2 surface and the g-C_3N_4 layer to increase absorption in the visible-light region *via* surface plasmon resonance, whilst the interface between Ag/TiO_2 and g-C_3N_4 stimulated the direct migration of photo-induced electrons from g-C_3N_4 to Ag/TiO_2, which was conducive to suppressing the recombination of electron–hole pairs. These results show that the performance of ss-DSSCs was significantly enhanced after modification with g-C_3N_4 and Ag, suggesting that heterostructured g-C_3N_4/Ag/TiO_2 composites can provide high photoelectric conversion through an effective electron transfer process.

Introduction

Dye-sensitized solar cells (DSSCs) are a promising alternative for photovoltaic technology and have gained widespread attention in recent years because of their low cost of manufacture, ease of fabrication, and tunable optical properties.[1,2] DSSCs are based on light-absorbing dye sensitizer attached to a TiO_2 layer that collects photo-generated electrons from the dye molecules. Some electrochemical DSSCs, through the molecular engineering of porphyrin sensitizers, can achieve a maximum energy conversion efficiency of more than 13%.[3] However, the liquid electrolytes can cause potential problems such as the instability of the DSSCs, particularly when the devices are fabricated with flexible substrates, resulting in corrosion and the potential electrolyte leakage from the DSSCs.[4–6] In recent years, researchers have found alternatives to liquid electrolytes, such as solid-state hole transport materials (HTMs), and the use of HTMs can overcome the above-mentioned problems such as electrolyte leakage.[7,8] The HTM layer plays an important role in regenerating the oxidized state of the light absorber in solid-state DSSCs (ss-DSSCs), and it also boosts hole transport to the counter-electrode in the solar cells, thus making it an essential part for efficient photoelectric performance.[9,10] Among numerous HTMs, spiro-OMeTAD (2,2′,7,7′-tetrakis-(*N*,*N*-di-*p*-methoxyphenylamine)-9,9′-spirobifluorene) is one of the most widely used HTMs, and has been attracting increasing attention.[7]

The ss-DSSCs made with spiro-OMeTAD have been optimized to achieve an efficiency of 7.7% using spiro-OMeTAD that has been doped with a cobalt complex.[11] Nevertheless, to date, the achieved efficiency for popular ss-DSSCs still remains in the low range of efficiency.[12,13] Some researchers tried to use thicker TiO_2 films for ss-DSSCs, which allow higher dye loading so that high efficiencies can be achieved by improving the light absorbance. However, in ss-DSSCs, thicker films are by no means sufficient for attaining a higher efficiency due to the fast recombination caused by the single-structured TiO_2 films.[14,15] This indicates that it is necessary to modify the photo-anode films to improve the efficiency for ss-DSSCs. Our previous study indicated that the modification with graphene can significantly reduce the band-gap of TiO_2 microspheres and greatly boost the electron transport within the photoanode.[16] Consequently, the conversion efficiency of the devices was greatly enhanced in DSSCs. Latterly, graphite carbon nitride (g-C_3N_4) has also drawn increasing attention in the field of visible-light photocatalysis and DSSCs.[17–20] g-C_3N_4 and graphene have a very similar layered structure, which allows them to form a thin layer like graphene on the surface of TiO_2 nanoparticles. Owing to the polymeric nature of g-C_3N_4, a thin g-C_3N_4 layer can easily be tuned by simply changing the amount of the

[a]*Key Laboratory of Advance Technologies of Materials, Ministry of Education, School of Materials Science and Engineering, Southwest Jiaotong University, Chengdu 610031, P. R. China. E-mail: jwang@swjtu.edu.cn; Fax: +86 28 87634649; Tel: +86 27 87634649*

[b]*School of Science and Engineering, Teesside University, Middlesbrough TS1 3BA, UK*

as-prepared precursor. In addition, g-C_3N_4 possesses a high chemical and thermal stability, and can be easily prepared by a simple thermal condensation from low-cost nitrogen rich raw materials. More importantly, g-C_3N_4 has more negative CB positions than TiO_2,[21] which may restrict the migration of photo-generated electrons effectively. However, in terms of visible-light irradiation, TiO_2 can only generate electrons, which results in a slow electron transfer from g-C_3N_4 to TiO_2 and a relatively high recombination of electron–hole pairs.[20] Accordingly, apart from the improvement of light absorption and electron transport, retarding such recombination is another effective avenue to further improve the performance of the ss-DSSCs. To overcome the fast recombination of electron–hole pairs, a considerable amount of research has been conducted on a hybrid modification of a noble metal and a semiconductor.[22,23] In the case of Ag/TiO_2 composites, Ag can serve as an electron sink to facilitate the transfer of interfacial electrons in the composite. Moreover, the composite can strongly absorb visible light due to the surface plasmon resonance of Ag.[24,25]

In this study, a ternary composite of g-C_3N_4/Ag/TiO_2 nanoparticles was prepared and applied in ss-DSSCs to enhance the performance. The effect of g-C_3N_4 and Ag on the performance of cell devices was investigated.

Experimental

Materials

Urea ($CO(NH_2)_2$, 99.0%), concentrated hydrochloric acid (HCl, 36.0–38.0%), concentrated sulfuric acid (H_2SO_4, 98.0%) and polyethylene glycol (PEG, M_w = 2000) were purchased from Chengdu Kelong Chemical Reagent Co., China. Titanium diisopropoxide bis(acetylacetonate) (75 wt% in isopropanol), ethyl cellulose (EC) and lithium bis(trifluoromethylsulphonyl)imide (Li-TFSI, 99%) were purchased from Sigma-Aldrich. Acetonitrile (99.8%), chlorobenzene (99%) and 4-*tert*-butylpyridine (TBP, 96%) were purchased from TCI. Silver nitrate ($AgNO_3$, ≥99.0%) and Zn powder (99.9%) were obtained from Sinopharm Chemical Reagent Co. Ltd. All reagents were of analytical grade and used without further purification.

Preparation of g-C_3N_4 sheets

Graphite-like carbon nitride (g-C_3N_4) nanosheets were prepared according to a method reported previously.[26] Urea was used as a precursor for g-C_3N_4. Specifically, 10.0 g of urea was calcined at 550 °C for 2 h at a heating rate of 5 °C min^{-1} in a muffle furnace. The obtained light yellow g-C_3N_4 agglomerate was ground into a powder. 1.0 g of the g-C_3N_4 powder was treated using a post processing with HCl (6 M, 50 mL) for 6 h at room temperature for protonation.[27] Before being filtered, the g-C_3N_4 suspension solution was diluted in 500 mL of deionized water. Subsequently, the protonated g-C_3N_4 was rinsed with deionized water until neutral pH and dried in air. 50 mg of the as-prepared protonated g-C_3N_4 powder was dispersed in 50 mL of deionized water by ultrasonication to obtain a well-dispersed suspension solution with a 1 mg mL^{-1} concentration.

Preparation of the g-C_3N_4/Ag/TiO_2 composite

The TiO_2 nanoparticles (P25, Degussa, 300 mg) were ultrasonically dispersed in 200 mL of deionized water. Then, 1.0 mL of a 5% polyethylene glycol (PEG, M_w = 2000) aqueous solution was added and stirred for another 10 min to form the suspension solution of TiO_2 nanoparticles. In order to deposit silver onto the surface of the TiO_2 nanoparticles, a photo-deposition method was used as follows: 3.5 mL of $AgNO_3$ solution (2.754 mg mL^{-1}) was added to the suspension solution of TiO_2 nanoparticles. Then, the suspension solution was irradiated under a Xe lamp (PLS-SXE300) at a 100 mW cm^{-2} illumination intensity for 60 min. The theoretical value of Ag-loading amount was 2 wt%.[28,29] For comparison, g-C_3N_4/TiO_2 composites were prepared *via* the same process but without the deposition of Ag. For further wrapping g-C_3N_4 on the TiO_2 and Ag/TiO_2 nanoparticles, a certain amount (9, 15 and 24 mL) of the protonated g-C_3N_4 suspension solution (1 mg mL^{-1}) was added and allowed to react at 70 °C for 60 min. The theoretical wrapping amount of g-C_3N_4 was 3, 5 and 8 wt%, and the obtained products without silver were denoted as CT-3, CT-5, CT-8, respectively, whilst those with silver were denoted as CT-*n*/Ag (where *n* is the amount of g-C_3N_4). The resulting suspension solution was filtered, rinsed with deionized water three times and then dried overnight at 60 °C in a vacuum oven.

Fabrication of the ss-DSSCs

Fluorine-doped tin oxide (FTO)-coated conductive glass substrates (NSG, 8 Ω sq^{-1}) with the desired dimensions (1.2 cm × 1.2 cm) were patterned by etching with Zn powder and 2 M HCl aqueous solution. The etched substrates were cleaned with detergent and subsequently rinsed with ethanol and isopropanol in an ultrasonic bath for 15 min, respectively, and then dried for use. A dense compact layer of TiO_2 was coated onto the FTO glass substrates by spin-coating at 2500 rpm for 40 s with a solution of 200 mM titanium diisopropoxidebis(acetylacetonate) in ethanol, and then sintered at 450 °C for 30 min in air. Thereafter, nanoporous films made of different nanoparticles of TiO_2/Ag/g-C_3N_4, TiO_2/g-C_3N_4 and pure TiO_2 were deposited on the TiO_2 compact layer by spin-coating using self-prepared pastes with the abovementioned compositions.[30] The pastes were prepared using the following procedure: 1.6 g of the abovementioned nanoparticles, 0.35 g of EC (46 cps), 0.45 g of EC (10 cps), 6.5 g of terpineol and 20 mL of anhydrous ethanol were mixed, and the mixture was ball-milled for 2 h to obtain a paste. The obtained paste was spun onto the TiO_2 compact layer at 3000 rpm for 30 s, and then sintered at 450 °C for 30 min in air. For comparison, pastes with four different weight ratios of g-C_3N_4 to TiO_2 were prepared following the same method. Finally, the obtained TiO_2/g-C_3N_4 films were soaked in a 40 mM $TiCl_4$ aqueous solution at 70 °C for 30 min and then were annealed at 450 °C for 15 min. After that, the dye was loaded by immersing the TiO_2 anode in a 0.3 mM dye N719 ethanol solution overnight. The HTM was deposited onto the dye-coated TiO_2 films through spin-coating a spiro-OMeTAD solution at 4000 rpm for 30 s. The spiro-OMeTAD solution was prepared by dissolving 72.3 mg of

spiro-OMeTAD, 28.8 μL of TBP, and 17.5 μL of Li-TFSI solution (520 mg Li-TFSI in 1 mL acetonitrile) in 1 mL of chlorobenzene.[31] Device fabrication process was conducted by depositing a 120 nm thick Ag film on top of the HTM layer. The 9 mm^2 active area of the devices was determined using a 3 mm × 3 mm black mask.

Characterization

The phase analysis of the as-prepared samples was carried out using an X-ray diffractometer (XRD) (Philips X'Pert PRO) under Cu Ka radiation (k = 1.5418 Å) from 15° to 75° of 2θ. Surface morphologies and microstructures of the g-C_3N_4/TiO_2 and g-C_3N_4/Ag/TiO_2 composites were characterized using field emission scanning electron microscopy (FESEM, JSM-7500F, JEOL, Japan) and high-resolution transmission electron microscopy (HRTEM) at a 200 kV accelerating voltage. The UV-vis diffuse reflectance spectra of the as-prepared samples were obtained with a UV-vis spectrophotometer (UV-2550, Shimadzu, Japan) and $BaSO_4$ was used as a reflectance standard. The Fourier transform infrared spectra (FT-IR) were obtained with a FT-IR spectrometer (Shimadzu Corp., Tokyo, Japan).

Electrochemical impedance spectroscopy (EIS) measurements were conducted using a computer-controlled electrochemical workstation with impedance analyzer (CIMPS-2, Zahner, Germany). The measurements were carried out by applying a 10 mV ac signal over a frequency range of 0.1 Hz to 100 kHz under illumination of AM 1.5G at the applied bias of open circuit voltage. The photovoltaic parameters of ss-DSSCs under simulated AM 1.5G illumination with a light intensity of 100 mW cm^{-2} provided by a 150 W xenon arc lamp (XBO 150 W/CROFR, OSRAM, USA) were measured with a potentiostat (CIMPS-2, Zahner, Germany). The active area of ss-DSSCs was 9 mm^2. The power conversion efficiency (PCE) was calculated according to the following equations:

$$\text{PCE}\ (\%) = \frac{J_{SC} \times V_{OC} \times \text{FF}}{P_{in}} \times 100\% \quad (1)$$

$$\text{FF} = \frac{P_{max}}{J_{SC} \times V_{OC}} \quad (2)$$

where V_{OC},J_{SC}, and FF, respectively, indicate open circuit voltage, short circuit current density, and fill factor; P_{in} is the energy of the incident monochromatic light; P_{max} is the maximum output power. The incident-photon-to-current conversion efficiency (IPCE) spectra were obtained with an IPCE measurement system (PEC-S20, Peccell Technologies Inc., Japan).

Results and discussion

Phase structures and FT-IR analysis

The XRD patterns of the as-prepared samples are shown in Fig. 1A. It can be seen that pure TiO_2 and TiO_2 composites with different components exhibited similar diffraction patterns. The diffraction peaks indicated the existence of the mixed phase of anatase and rutile, which are ascribed to pure TiO_2 (P25).[32] For the g-C_3N_4 sample, the peak appearing at a 2θ value of 27.4° corresponds to the (002) crystal plane, which is ascribed to the interlayer stacking of aromatic segments. However, it can be noted that no characteristic peaks of g-C_3N_4 and Ag were observed in either g-C_3N_4/TiO_2 or g-C_3N_4/Ag/TiO_2 composites. The reason for this might be attributed to the low amount of g-C_3N_4 and Ag, as well as a poor crystallization of g-C_3N_4 on the surface of the TiO_2 composites. Another reason might be that the main peak of g-C_3N_4 at a 2θ of 27.4° and the peak of Ag at a 2θ of 38.1° might have overlapped with the peak of TiO_2 at the same 2θ position so that it would have been hard to tell the difference between them.

Fig. 1B shows the FT-IR spectra of the pure TiO_2 nanoparticles, g-C_3N_4 powder, g-C_3N_4/TiO_2 composites and g-C_3N_4/Ag/TiO_2 composites. For pure TiO_2 and composites, the spectra shows a wide absorption peak (500 to 700 cm^{-1}) attributed to Ti–O and Ti–O–Ti stretchings, whilst the peak at 1631 cm^{-1} is associated with the bending vibration of surface O–H. The absorption peak at 1638 cm^{-1} can be ascribed to the C–N heterocycle stretching vibration modes,[20] whereas the four strong absorption peaks at 1252, 1328, 1415 and 1572 cm^{-1} can be ascribed to the typical C–N stretching vibration modes.[33] The peak at 808 cm^{-1} is associated with the characteristic breathing mode of triazine units.[21] The g-C_3N_4/TiO_2 composites showed similar absorption peaks to those of pure TiO_2 nanoparticles. In addition, all of the main characteristic peaks of g-C_3N_4 and TiO_2 could also be observed in g-C_3N_4/Ag/TiO_2 composites.

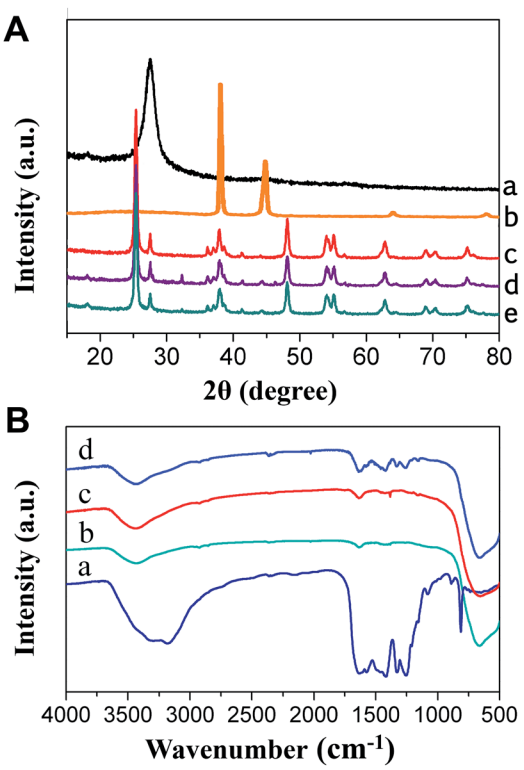

Fig. 1 (A) XRD patterns of (a) g-C_3N_4 powder, (b) Ag nanoparticles, (c) TiO_2, (d) g-C_3N_4/TiO_2 composite, (e) g-C_3N_4/Ag/TiO_2 (CT-5/Ag) composite; (B) FT-IR patterns of (a) g-C_3N_4 powder, (b) TiO_2, (c) g-C_3N_4/TiO_2 composite, (d) CT-5/Ag composite.

Morphology characterizations

In order to further investigate the multilayered structure of the g-C_3N_4/Ag/TiO_2 composites, TEM characterization was performed. Fig. 2A showed a TEM image of the as-prepared g-C_3N_4/Ag/TiO_2 composite. It can be seen that the components, with a different recognizable crystal structure, are firmly held in place within the sample material and the size is in the range of 20–30 nm. A three-layer composite structure, having the outer layer of g-C_3N_4 (with a thickness of about 2.5 nm), the interlayer of Ag particles and the inlayer of TiO_2 particles, was clearly observed. The Ag nanoparticles loaded onto the TiO_2 nanoparticles had a size of about 10 nm. The corresponding HRTEM image from a single composite (Fig. 2B) showed that the lattice spacing was 0.35 nm and 0.23 nm, respectively, which can be attributed to the (101) planes of anatase TiO_2 and the (111) planes of Ag. The corresponding SAED pattern, as shown in the inset of Fig. 2B, further demonstrated a polycrystalline ternary composite structure for the g-C_3N_4/Ag/TiO_2 nanoparticles. Such structural feature is beneficial for diminishing the direct contact between TiO_2 and g-C_3N_4 so as to further block the electron–hole recombination.

To investigate whether or not surface chemical modification of the composite nanoparticles had been achieved, elemental analysis of the photoanode film containing g-C_3N_4 and silver was conducted using scanning electron microscopy-energy dispersive X-ray spectroscopy (SEM-EDS). The SEM-EDS images confirmed the presence of C, N, O, Ag and Ti in the film (Fig. 3). By SEM-EDS, the content and distribution of the chemical constituents could be estimated at the subnanometre level. The SEM-EDS mapping for each element shows that g-C_3N_4 and Ag were uniformly distributed in the whole photoanode film.

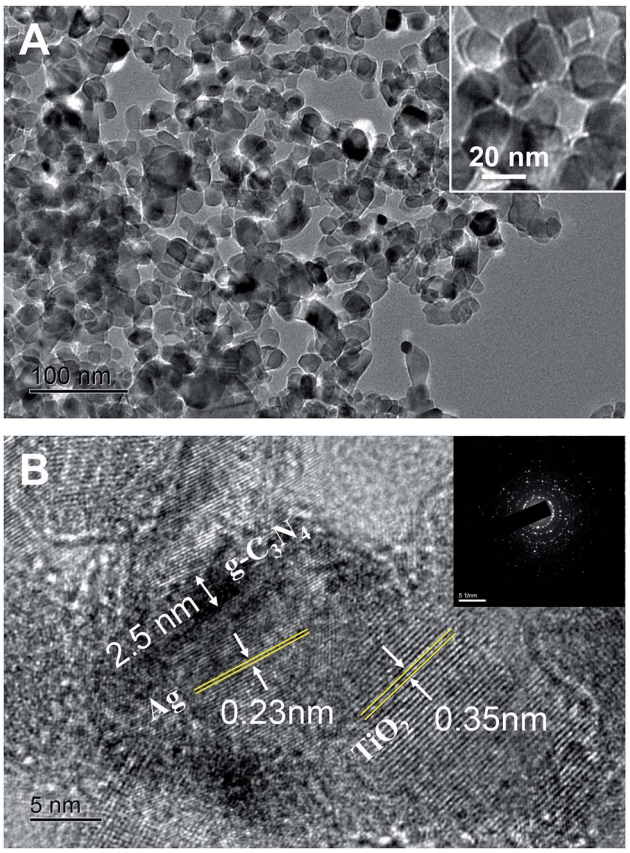

Fig. 2 (A) TEM and (B) HRTEM images of the as-prepared g-C_3N_4/Ag/TiO_2 (CT-5/Ag) composite nanoparticles (inset: SAED pattern of the same composite nanoparticles).

UV-vis diffuses reflectance spectra

The UV-vis absorbance properties of the as-prepared samples were analyzed by UV-vis diffuse reflectance spectroscopy. Fig. 4A shows the UV-vis diffuse reflectance spectra of the CT-5 and CT-5/Ag composite nanoparticles, together with those of pure TiO_2 (CT-0) and protonated g-C_3N_4. For the pure TiO_2 particles, the basal absorption occurred at a wavelength region below 380 nm, whereas the absorption wavelength region for protonated g-C_3N_4 was below 500 nm. For the g-C_3N_4-modified TiO_2 particles, the absorption wavelength region was wider, distinctly in the visible light region. When compared with pure TiO_2 particles, the CT-5 composites showed an additional absorption in the 360–370 nm region and the absorption edge occurred at a wavelength of about 410 nm, which might be due to the existence of g-C_3N_4 on the surface of the TiO_2 particles.[34] g-C_3N_4/Ag/TiO_2 composites showed prominent visible-light absorption, which might be attributed to the surface plasmon resonance (SPR) of the loading Ag, further confirming the formation of Ag nanoparticles.[35] The band gap energies of semiconductors were estimated by the Kubelka–Munk transformation, $\alpha h\nu = A(h\nu - E_g)^{1/2}$, where α represents the absorption coefficient, ν is the light frequency, E_g is the band gap energy, A is a constant and n depends on the characteristics of the transition in a semiconductor. Thus, as shown in Fig. 4B, the E_g of pure TiO_2 nanoparticles, CT-5 composites, g-C_3N_4 powder and CT-5/Ag composites were calculated to be 3.21, 3.10, 2.74 and 2.66 eV, respectively. It is evident that the introduction of Ag and g-C_3N_4 into TiO_2 nanoparticles greatly decreased the band gap, which would lower the required energy for photo-induced electrons, thus enhancing incident light utilization efficiency in the longer wavelength region.

Effects of g-C_3N_4 and Ag on the performance of the ss-DSSCs

Fig. 5 shows the photoelectric performances of the ss-DSSCs, which were measured under simulated AM 1.5 solar spectrum irradiated at 100 mW cm^{-2}. Table 1 shows the performance parameters of the ss-DSSC devices. It can be seen from Fig. 5A that the PCE of the ss-DSSC fabricated with pure TiO_2 (P25, CT-0) for the photoanode was just 3.72%, whereas the PCEs for ss-DSSCs with CT-3, CT-5 and CT-8 were 4.65%, 5.34% and 4.27%, respectively. It is clear that the use of the g-C_3N_4 modified TiO_2 significantly improved the PCE of the devices. All the CT-based ss-DSSCs exhibited higher efficiency than the ss-DSSCs fabricated with pure TiO_2. Among them, the CT-5-based ss-DSSC exhibited the best performance, with J_{SC} = 11.76 mA·cm^{-2}, V_{OC} = 0.708 V, and FF = 0.641, which conforms to a notably high PCE of 5.34%, representing an improvement of about 43% over the ss-DSSC having only P25 as the photoanode material.

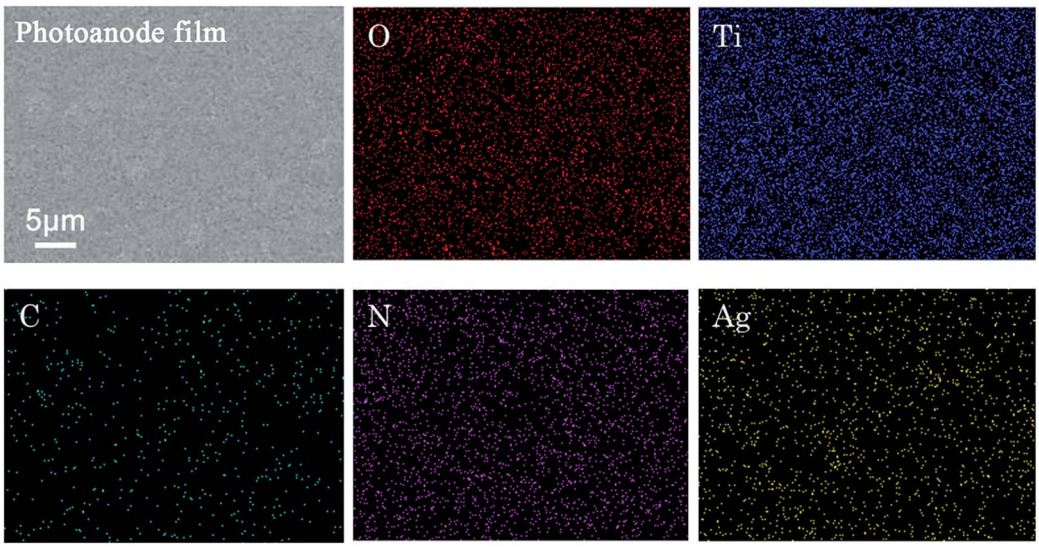

Fig. 3 SEM surface morphology and EDS mapping images of the photoanode film (prepared with CT-5/Ag composite nanoparticles).

However, it follows that it is not true that more the g-C_3N_4 wrapped on the TiO_2 nanoparticles, the better the performance of ss-DSSCs. It is well known that besides the electron concentration, the electron diffusion is also an essential factor that can affect the conversion efficiency of solar cells. Hence, the overloading of g-C_3N_4 might partially affect the effective connection between TiO_2 nanoparticles, thus interrupting the fast transport of electrons from TiO_2 to FTO substrates and causing the decrease of J_{SC}. Due to the co-effect of both electron concentration and electron diffusion, the as-prepared ss-DSSCs showed a first-increase-then-decrease tendency of performance with the increase of g-C_3N_4 loading amount. For the g-C_3N_4 and Ag co-modified ss-DSSCs, the result (Fig. 5B) shows that when g-C_3N_4 and Ag were simultaneously applied as the photoanode material, the obtained PCE for the ss-DSSC was 6.22%, which was the highest efficiency among all as-prepared ss-DSSCs so far, and was about 1.7 times the PCE value obtained for a ss-DSSC with pure TiO_2 (with an efficiency of 3.72%). Moreover, it can be seen that the photocurrent density improved from 8.63 to 12.68 mA cm^{-2}. The enhanced efficiency of these ss-DSSCs might be explained by the role of Ag particles. Some researchers reported that Ag can reduce the surface trap states of TiO_2 and Ag nanoparticles can play a dual role in enhancing both the absorption coefficient of the dye and the optical absorption *via* surface plasmon resonance.[36–38] In addition, they can serve as an electron sink for photo-induced charge carriers, which improves the interfacial charge transfer process, and minimizes charge recombination,[38] thereby enhancing the electron transfer process in ss-DSSCs and improving ss-DSSC efficiency.

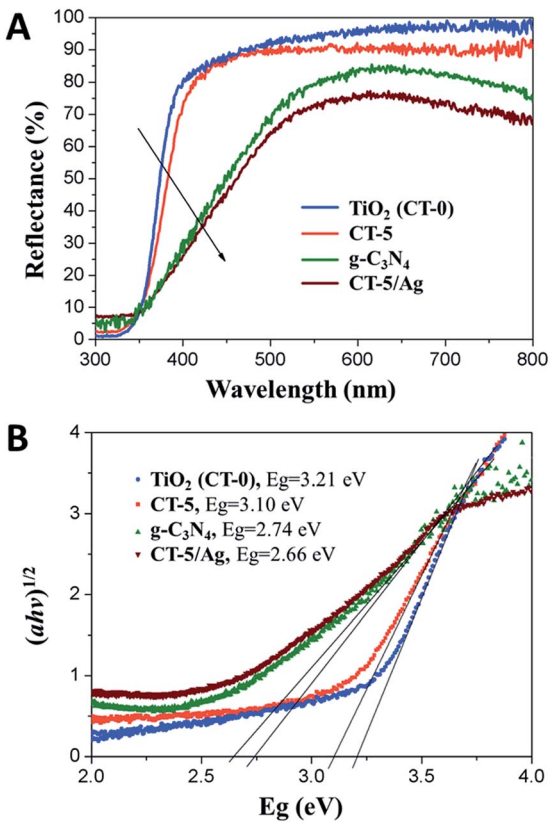

Fig. 4 (A) UV-vis diffuse reflectance spectra of pure TiO_2 (CT-0), CT-5 composite, g-C_3N_4 powder and CT-5/Ag composite and (B) their corresponding Kubelka–Munk transformed reflectance spectra.

To further elucidate the effects of g-C_3N_4 and Ag on the performance of the solar cells, electrochemical impedance spectroscopy (EIS) measurements were performed to study the charge transfer resistance in the prepared solar cells (Fig. 5C). The EIS curves of all devices can be fitted through the ZSimpWin software, as shown in Fig. 5C and the data is shown in Table 2. The equivalent circuits were used to fit the kinetic parameters.[39] Higher frequency arcs corresponded to the hole transport, whereas lower frequency arcs corresponded to the electron transport and recombination. The fitted recombination (R_{ct}), electron transport (R_t), and hole transport resistance (R_h) were plotted against the open-circuit voltage. As

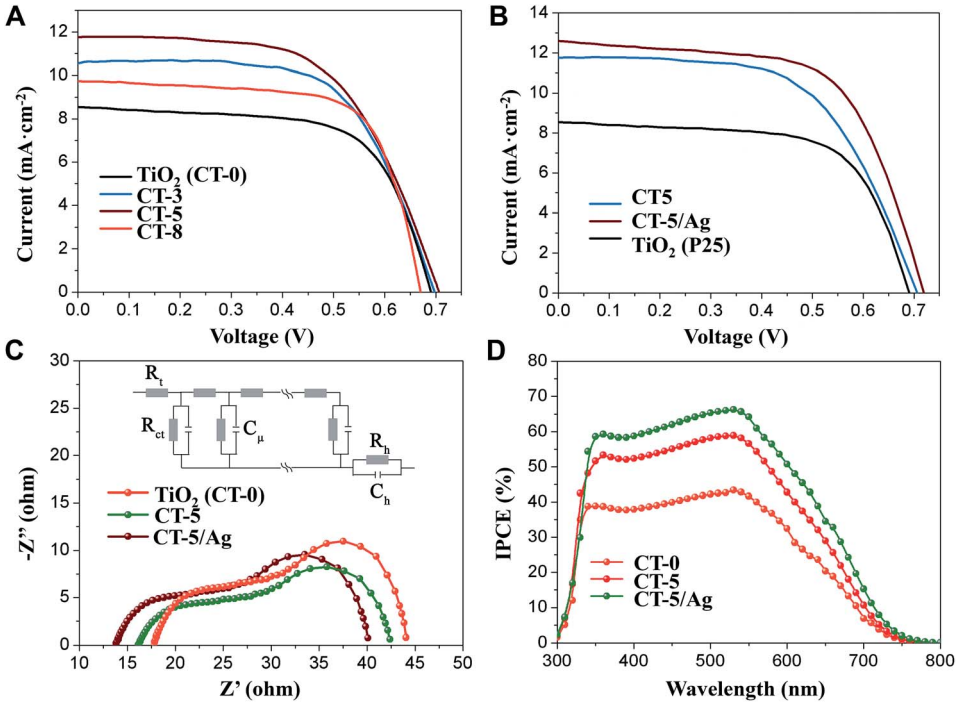

Fig. 5 (A) *I–V* characteristics of ss-DSSCs with pure P25 (CT-0), CT-3, CT-5 and CT-8, respectively; (B) *I–V* characteristics of ss-DSSCs without and with Ag and g-C_3N_4; (C) Nyquist plots and (D) IPCE spectra of ss-DSSCs with CT-0, CT-5 and CT-5/Ag composite electrodes, respectively.

the charge separated at the TiO_2/dye/HTM interface, the recombination between electrons in TiO_2 and holes in spiro-OMeTAD became the dominant loss mechanism in ss-DSSCs. Snaith *et al.*[40] have reported that the recombination occurred by means of the quantum mechanical tunnelling of electrons from TiO_2 through the dye to recombine with holes in HTMs. The comparison of the devices with CT-0, CT-5 and CT-5/Ag showed that the recombination was impeded for those devices with g-C_3N_4. This result might be because the g-C_3N_4 could increase the separation distance between electrons in dye/TiO_2 and holes in spiro-OMeTAD.[41] The recombination retardation decreased with the incorporation of g-C_3N_4 and Ag in the photo-anode.

Table 1 Solar cell performance parameters

Sample	J_{SC} (mA cm^2)	V_{OC} (V)	FF	PCE (%)
TiO_2	8.63	0.673	0.640	3.72
CT-3	10.58	0.698	0.631	4.65
CT-5	11.76	0.708	0.641	5.34
CT-8	9.77	0.667	0.655	4.27
CT-5/Ag	12.68	0.715	0.686	6.22

Table 2 EIS data of the devices[a]

Sample	R_{rec} (Ω cm^{-2})	C_μ (F)	τ_e (ms)
TiO_2	14.1	3.63×10^{-4}	5.11
CT-5	12.2	6.41×10^{-4}	7.82
CT-5/Ag	11.6	1.56×10^{-3}	18.09

[a] R_{rec} (the recombination resistance); C_μ (the chemical capacitance); τ_e (electron lifetime; the values were calculated from the fitting data of EIS measurements by means of reference[42]).

Fig. 5D displays the comparison of IPCE curves for the ss-DSSCs based on different composites for the photoanodes. Generally speaking, the photocurrent onset of the TiO_2/dye, CT-5/dye and CT-5/Ag/dye electrodes as measured from the IPCE spectra is consistent with the onset of optical light absorption. It can be estimated from the UV-vis diffuse reflectance spectra that the cascade CT-5/Ag/dye electrode has not only a broader light harvesting range, when compared with the rest, but also higher IPCE values. The reason for this might be that the reduced charge recombination results in a more efficient charge collection from the g-C_3N_4 nanosheets and Ag nanoparticles, thus increasing the IPCE after the modification with g-C_3N_4 or Ag nanoparticles. The highest IPCE (64%) was recorded for the ss-DSSCs modified with both g-C_3N_4 and Ag at a wavelength of 540 nm. As we know, the light-harvesting efficiency (LHE) can be calculated by the following formula: $LHE = 1 - 10^{-A}$, where A is the absorbance at a given wavelength.[43,44] The LHE and the absorbed photon-to-current efficiency (APCE) data are also provided as shown in Fig. 6; the APCE data were obtained from the corresponding LHE and IPCE data. Consequently, it provided an evidence for the reliability of the increase in J_{SC}, with higher values in the long wavelength region for those devices having g-C_3N_4 and g-C_3N_4/Ag, which is an indicator of reduced carrier recombination. This was consistent with the corresponding photo-voltaic performance and it is reasonable that the CT-5 sample possessed the optimal loading amount of g-C_3N_4, which would act as

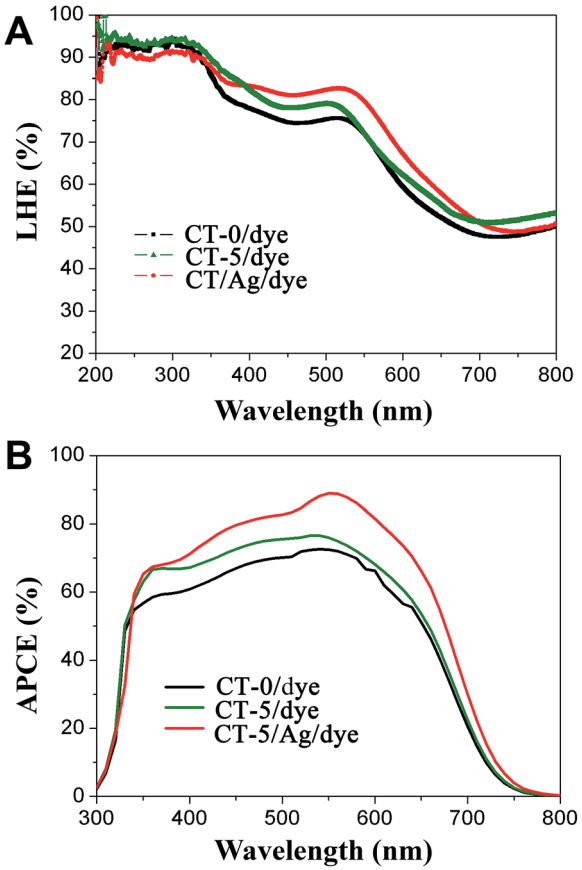

Fig. 6 (A) LHE spectra of TiO_2/dye, CT-5/dye and CT-5/Ag/dye (B) APCE spectra derived from the IPCE and LHE.

a blocking layer to suppress the backward recombination of electrons from TiO_2 and dye.

On the basis of the above results, the enhanced performance mechanism for the g-C_3N_4/Ag/TiO_2 composites was proposed and schematically exhibited in Fig. 7. Herein, the optimal loading of g-C_3N_4 on the TiO_2 surface plays a crucial role in improving the performance of the devices, which can serve as a block layer to retard the electron backward recombination. g-C_3N_4 has more negative CB positions as compared with that of TiO_2, and thus, electrons in the CB positions of TiO_2 cannot transfer to g-C_3N_4.

Conversely, the electrons from the CB positions of g-C_3N_4 can easily transfer to the CB positions of TiO_2. Accordingly, the thin g-C_3N_4 layer on the TiO_2 surface can effectively increase the electron concentration in the photoanode, thus resulting in an enhanced performance. However, a higher amount of g-C_3N_4 can prominently decrease the electron transport from the TiO_2 to the FTO substrate, and might partially cut off the effective connection among TiO_2 nanoparticles, which can interrupt the fast transport of electrons from TiO_2 to FTO substrates, thus resulting in the increase of electron transport resistance and subsequently the decrease of J_{SC}.

Ag nanoparticles deposited on the TiO_2 surface also play a crucial role as a bridge for electron conduction by which the electrons can transfer to TiO_2, and electron–hole pair separation in g-C_3N_4 becomes more efficient due to the formed Schottky barrier at the interface of the Ag and TiO_2 nanoparticles.[45] Alternatively, the surface plasmon resonance of Ag nanoparticles can promote visible-light absorption.[25] As a result, the photovoltaic performance of the ss-DSSCs can be further promoted.

Conclusion

g-C_3N_4/Ag/TiO_2 nanocomposites were successfully prepared *via* a facile route and applied in the ss-DSSCs photoanodes. The ss-DSSCs based on the g-C_3N_4/Ag/TiO_2 composite achieved a significant improvement of photoelectric efficiency compared with that of the ss-DSSC with pure TiO_2. The PCE of the

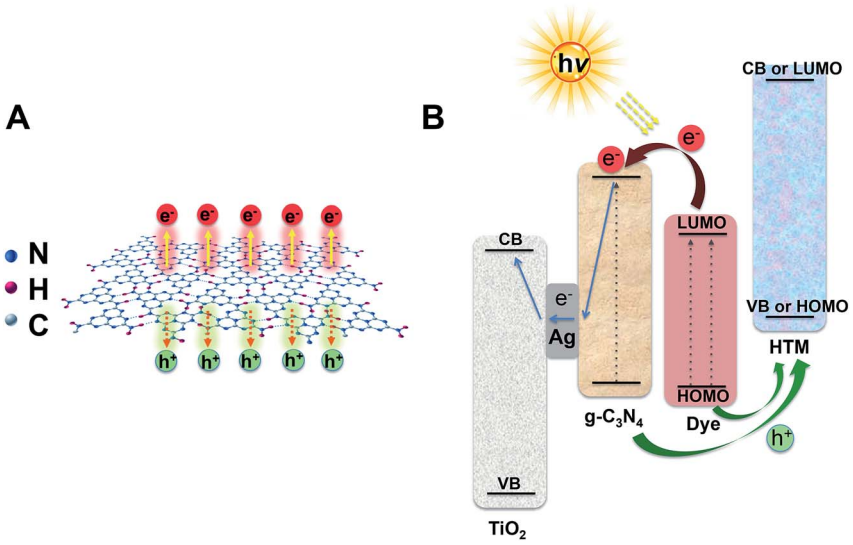

Fig. 7 (A) Schematic for g-C_3N_4 to separate the photo-generated electrons and holes; (B) schematic diagram of the electron transfer process in ss-DSSCs based on the photoanode with g-C_3N_4 and Ag co-modified TiO_2 composites.

ss-DSSCs improved near 66% at an optimal loading amount of about 2.0 wt% Ag and 5.0 wt% g-C_3N_4. The enhancement of the solar cell performance was ascribed to the g-C_3N_4 and Ag on the TiO_2 surface, which could not only contribute additional electrons that increase the electron concentration in the photoanodes, but also suppress the backward recombination of electrons from TiO_2 and the hole transporting layer.

Acknowledgements

This work was supported by the National Natural Science Foundation of China (No. 51072167 and 31370966) and the Fundamental Scientific Research Funds for Central Universities (SWJTU11CX058).

Notes and references

1 B. O'Regan and M. Grätzel, A low cost, high-efficiency solar cell based on dye-sensitized colloidal TiO_2 films, *Nature*, 1991, **353**, 737–740.

2 M. Motlak, N. A. M. Barakat, M. S. Akhtar, A. G. El-Deen, M. Obaid, C. S. Kim, K. A. Khalil and A. A. Almajid, High-efficiency dye-sensitized solar cells based on nitrogen and graphene oxide co-incorporated TiO_2 nanofibers photoelectrode, *Chem. Eng. J.*, 2015, **268**, 153–161.

3 S. Mathew, A. Yella, P. Gao, R. Humphry-Baker, B. F. Curchod, N. Ashari-Astani, I. Tavernelli, U. Rothlisberger, M. K. Nazeeruddin and M. Grätzel, Dye-sensitized solar cells with 13% efficiency achieved through the molecular engineering of porphyrin sensitizers, *Nat. Chem.*, 2014, **6**, 242–247.

4 Y. L. Fang, Q. Wang, J. G. Huang and T. Wu, Enhanced pore filling of spiro-OMeTAD by enlarging the porosity of TiO_2 films and its effects on the photovoltaic performance of ss-DSCs, *Appl. Phys. A*, 2015, **118**, 1339–1346.

5 M. Chen and L. L. Shao, Review on the recent progress of carbon counter electrodes for dye-sensitized solar cells, *Chem. Eng. J.*, 2016, **304**, 629–645.

6 P. Wang, Q. Dai, S. M. Zakeeruddin, M. Forsyth, D. R. MacFarlane and M. Grätzel, Ambient temperature plastic crystal electrolyte for efficient, all-solid-state dye-sensitized solar cell, *J. Am. Chem. Soc.*, 2004, **126**, 13590–13591.

7 L. Yang, B. Xu, D. Bi, H. Tian, G. Boschloo, L. Sun, A. Hagfeldt and E. M. Jahansson, Initial light soaking treatment enables hole transport material to outperform spiro-OMeTAD in solid-state dye-sensitized solar cells, *J. Am. Chem. Soc.*, 2013, **135**, 7378–7385.

8 B. Xu, D. Q. Bi, Y. Hua, P. Liu, M. Cheng, M. Grätzel, L. Kloo, A. Hagfeldt and L. C. Sun, A low-cost spiro[fluorene-9,90-xanthene]-based hole transport material for highly efficient solid-state dye-sensitized solar cells and perovskite solar cells, *Energy Environ. Sci.*, 2016, **9**, 873–877.

9 P. Docampo, S. Guldin, T. Leijtens, N. K. Noel, U. Steiner and H. J. Snaith, Lessons learned: from dye-sensitized solar cells to all-solid-state hybrid devices, *Adv. Mater.*, 2014, **24**, 4013–4030.

10 S. Ameen, M. S. Akhtar, H. K. Seo and H. S. Shin, Towards design of metal oxide free perovskite solar cell paradigm: materials processing and enhanced device performance, *Chem. Eng. J.*, 2015, **281**, 599–605.

11 J. Burschka, A. Dualeh, F. Kessler, E. Baranoff, N. L. Cevey-Ha, C. Yi, M. K. Nazeeruddin and M. Grätzel, Tris(2-(1*H*-pyrazol-1-yl)pyridine)cobalt(III) as p-type dopant for organic semiconductors and its application in highly efficient solid-state dye-sensitized solar cells, *J. Am. Chem. Soc.*, 2011, **133**, 18042–18045.

12 T. T. Bui, S. K. Shah, M. Abbas, X. Sallenave, G. Sini, L. Hirsch and F. Goubard, Carbazole-based molecular glasses as hole-transporting materials in solid state dye-sensitized solar cells, *Chem. Nanostruct. Mater.*, 2015, **1**, 203–210.

13 M. Planells, A. Abate, D. J. Hollman, S. D. Stranks, V. Bharti, J. Gaur, D. Mohanty, S. Chand, H. J. Snaith and N. Robertson, Diacetylene bridged triphenylamines as hole transport materials for solid state dye sensitized solar cells, *J. Mater. Chem. A*, 2013, **1**, 6949–6960.

14 C. D. Bailie, E. L. Unger, S. M. Zakeeruddin, M. Grätzel and M. D. McGehee, Melt-infiltration of spiro-OMeTAD and thermal instability of solid-state dye-sensitized solar cells, *Phys. Chem. Chem. Phys.*, 2014, **16**, 4864–4870.

15 I. K. Ding, J. Melas-Kyriazi, N. J. Cevey-Ha, K. G. Chittibabu, S. M. Zakeeruddin, M. Grätzel and M. D. McGehee, Deposition of hole-transport materials in solid-state dye-sensitized solar cells by doctor-blading, *Org. Electron.*, 2010, **11**, 1217–1222.

16 H. Yan, J. Wang, B. Feng, K. Duan and J. Weng, Graphene and Ag nanowires co-modified photoanodes for high-efficiency dye-sensitized solar cells, *Sol. Energy*, 2015, **122**, 966–975.

17 J. X. Low, S. W. Cao, J. G. Yu and S. Wageh, Two-dimensional layered composite photocatalysts, *Chem. Commun.*, 2014, **50**, 10768–10777.

18 J. G. Yu, K. Wang, W. Xiao and B. Cheng, Photocatalytic reduction of CO_2 into hydrocarbon solar fuels over g-C_3N_4–Pt nanocomposite photocatalysts, *Phys. Chem. Chem. Phys.*, 2014, **16**, 11492–11501.

19 D. P. Wu, K. Cao, F. J. Wang, H. J. Wang, Z. Y. Gao, F. Xu, Y. M. Guo and K. Jiang, Two dimensional graphitic-phase C_3N_4 as multifunctional protecting layer for enhanced short-circuit photocurrent in ZnO based dye-sensitized solar cells, *Chem. Eng. J.*, 2015, **280**, 441–447.

20 Y. F. Chen, W. X. Huang, D. L. He, Y. Situ and H. Huang, Construction of heterostructured C_3N_4/Ag/TiO_2 microspheres with enhanced photocatalysis performance under visible-light irradiation, *ACS Appl. Mater. Interfaces*, 2014, **6**, 14405–14414.

21 J. Xu, G. X. Wang, J. J. Fan, B. S. Liu, S. W. Cao and J. G. Yu, g-C_3N_4 modified TiO_2 nanosheets with enhanced photoelectric conversion efficiency in dye-sensitized solar cells, *J. Power Sources*, 2015, **274**, 77–84.

22 S. Sakthivel, M. V. Shankar, M. Palanichamy, B. Arabindoo, D. W. Bahnemann and V. Murugesan, Enhancement of photocatalytic activity by metal deposition: characterisation

and photonic efficiency of Pt, Au and Pd deposited on TiO_2 catalyst, *Water Res.*, 2004, **38**, 3001–3008.

23 Z. K. Zheng, B. B. Huang, X. Y. Qin, X. Y. Zhang, Y. Dai and M. H. Whangbo, Facile *in situ* synthesis of visible-light plasmonic photocatalysts M@TiO_2 (M = Au, Pt, Ag) and evaluation of their photocatalytic oxidation of benzene to phenol, *J. Mater. Chem.*, 2011, **21**, 9079–9087.

24 C. S. Lan, K. H. Leong, S. Ibrahim and P. Saravanan, Graphene oxide and Ag engulfed TiO_2 nanotube arrays for enhanced electron mobility and visible-light-driven photocatalytic performance, *J. Mater. Chem. A*, 2014, **2**, 5315–5322.

25 Q. Xiao, S. Sarina, A. Bo, J. F. Jia, H. W. Liu, D. P. Arnold, Y. M. Huang, H. S. Wu and H. Y. Zhu, Visible light-driven cross-coupling reactions at lower temperatures using a photocatalyst of palladium and gold alloy nanoparticles, *ACS Catal.*, 2014, **4**, 1725–1734.

26 S. C. Yan, Z. S. Li and Z. G. Zou, Photodegradation performance of g-C_3N_4 fabricated by directly heating melamine, *Langmuir*, 2009, **25**, 10397–10401.

27 Y. J. Zhang, A. Thomas, M. Antonietti and X. C. Wang, Activation of carbon nitride solids by protonation: morphology changes, enhanced ionic conductivity, and photoconduction experiments, *J. Am. Chem. Soc.*, 2009, **131**, 50–51.

28 V. Iliev, D. Tomova, L. Bilyarska, A. Eliyas and L. Petrov, Photocatalytic properties of TiO_2 modified with platinum and silver nanoparticles in the degradation of oxalic acid in aqueous solution, *Appl. Catal., B*, 2006, **63**, 266–271.

29 F. A. He, J. T. Fan, F. Song, L. M. Zhang and H. Lai-Wa Chan, Fabrication of hybrids based on graphene and metal nanoparticles by *in situ* and self-assembled methods, *Nanoscale*, 2011, **3**, 1182–1188.

30 S. Ito, T. N. Murakami, P. Comte, P. Liska, C. Grätzel, M. K. Nazeeruddin and M. Grätzel, Fabrication of thin film dye-sensitized solar cells with solar to electric power conversion efficiency over 10%, *Thin Solid Films*, 2008, **516**, 4613–4619.

31 J. W. Lee, D. J. Seol, A. N. Cho and N. G. Park, High-efficiency perovskite solar cells based on the black polymorph of $HC(NH_2)_2PbI_3$, *Adv. Mater.*, 2014, **26**, 4991–4998.

32 H. L. Zhu, D. M. Chen, D. Yue, Z. H. Wang and H. Ding, *In situ* synthesis of g-C_3N_4–P25 TiO_2 composite with enhanced visible light photoactivity, *J. Nanopart. Res.*, 2014, **16**, 2632.

33 S. Kumar, T. Surendar, A. Baruah and V. Shanker, Synthesis of a novel and stable g-C_3N_4–Ag_3PO_4 hybrid nanocomposite photo-catalyst and study of the photocatalytic activity under visible light irradiation, *J. Mater. Chem. A*, 2013, **1**, 5333–5340.

34 M. K. Parvez, G. M. Yoo, J. H. Kim, M. J. Ko and S. R. Kim, Comparative study of plasma and ion-beam treatment to reduce the oxygen vacancies in TiO_2 and recombination reactions in dye-sensitized solar cells, *Chem. Phys. Lett.*, 2010, **495**, 69–72.

35 K. C. Lee, S. J. Lin, C. H. Lin, C. S. Tsai and Y. J. Lu, Size effect of Ag nanoparticles on surface plasmon resonance, *Surf. Coat. Technol.*, 2008, **202**, 5339–5342.

36 Z. H. Chen, C. M. Wang, L. H. Wang, C. Jiang and H. B. Zhu, Surface plasmonic resonance sensor by metal strip pair arrays, *Opt. Quantum Electron.*, 2013, **45**, 707–712.

37 K. H. Leong, B. L. Gan, S. Ibrahim and P. Saravanan, Synthesis of surface plasmon resonance (SPR) triggered Ag/TiO_2 photocatalyst for degradation of endocrine disturbing compounds, *Appl. Surf. Sci.*, 2014, **319**, 128–135.

38 J. W. Menezes, J. Ferreira, M. J. L. Santos, L. Cescato and A. G. Brolo, Large-area fabrication of periodic arrays of nanoholes in metal films and their application in biosensing and plasmonic-enhanced photovoltaics, *Adv. Funct. Mater.*, 2010, **20**, 3918–3924.

39 F. Fabregat-Santiago, J. Bisquert, L. Cevey, P. Chen, M. K. Wang, S. M. Zakeeruddin and M. Grätzel, Electron transport and recombination in solid-state dye solar cell with spiro-OMeTAD as hole conductor, *J. Am. Chem. Soc.*, 2009, **131**, 558–562.

40 H. J. Snaith, R. Humphry-Baker, P. Chen, I. Cesar, S. M. Zakeeruddin and M. Grätzel, Charge collection and pore filling in solid-state dye-sensitized solar cells, *Nanotechnology*, 2008, **19**, 424003.

41 I. K. Ding, N. Tetreault, J. Brillet, B. E. Hardin, E. H. Smith, S. J. Rosenthal, F. Sauvage, M. Grätzel and M. D. McGehee, Pore-filling of spiro-OMeTAD in solid-state dye sensitized solar cells: quantification, mechanism, and consequences for device performance, *Adv. Funct. Mater.*, 2009, **19**, 2431–2436.

42 J. Bisquert, F. Fabregatsantiago, I. Moraseró, G. Garciabelmonte and S. Giménez, Electron lifetime in dye-sensitized solar cells: theory and interpretation of measurements, *J. Phys. Chem. C*, 2009, **113**, 17278–17290.

43 Y. H. Lai, M. Kato, D. Mersch and E. Reisner, Comparison of photoelectrochemical water oxidation activity of a synthetic photocatalyst system with photosystem II, *Faraday Discuss.*, 2014, **176**, 199–211.

44 C. F. Chi, P. Chen, Y. L. Lee, I. P. Liu, S. C. Chou, X. L. Zhang and U. Bach, Surface modifications of CdS/CdSe co-sensitized TiO_2 photoelectrodes for solid-state quantum-dot-sensitized solar cells, *J. Mater. Chem.*, 2011, **21**, 17534–17540.

45 B. Chai, T. Y. Peng, J. Mao, K. Li and L. Zan, Graphitic carbon nitride (g-C_3N_4)–Pt–TiO_2 nanocomposite as an efficient photo-catalyst for hydrogen production under visible light irradiation, *Phys. Chem. Chem. Phys.*, 2012, **14**, 16745–16752.

